Optimal Multi-objective Robust Controller Design for Magnetic Levitation System

Assist. Prof. Dr. Hazem I. Ali[1] and Mr. Mustafa I. Abd[2]
[1,2]Control and Systems Engineering Department, University of Technology, Baghdad-Iraq
e-mail: hazem.i.ali@uotechnology.edu.iq, mustafa99r07@yahoo.com

Received: 7/9/2014

Accepted: 21/1/2015

Abstract- In this work, the design of three types of robust controllers is presented to control the magnetic levitation system. These controllers are: basic H_∞ controller, robust Genetic Algorithm (GA) based PID (GAPID) controller and robust Particle Swarm Optimization (PSO) based PID (PSOPID) controller. In the second and third controllers, the GA and PSO methods are used to tune the parameters of PID controller subject to multi-objective cost function (H_∞ constraints and time domain specifications). The use of GA and PSO methods is used to simplify the design procedure and to overcome the difficulty of the resulting high order controller of the basic H_∞ controller. The ability of the proposed controllers in compensating the system with a wide range of system parameters change is demonstrated by simulation using MATLAB 7.14.

Keywords: Magnetic levitation, Robust control, Multi-objective optimization, PSO, Optimal control.

1. Introduction

The magnetic levitation system is a method by which an object is suspended in the air with no support other than magnetic fields. The magnetic levitation systems have gained a great interest in the entire world due to their great practical importance in engineering fields. However; the magnetic levitation systems are characterized as unstable open loop, highly non linear and uncertain systems. Furthermore, these systems have high steady state error and they can be destabilized with a small change in system parameters. Magnetic levitation technology has an increase attention since it helps to eliminate friction losses due to mechanical contact. Some engineering applications include high-speed trains, magnetic bearings and high precision platforms. Magnetic levitation trains are recently tested and some lines are already available as for example in Shanghai. Magnetic bearings are used in turbines since low friction in the bearing itself. Already many turbines are used commercially where the rotating shaft is levitated with magnetic flux. Some other magnetic bearings applications include pumps, fans and other rotating machines [1].

There have been a number of works in the direction of the control of magnetic levitation system. Anupam et al [2] introduced an efficient controller to suspend the steel ball using an interval type-2 single input fuzzy logic controller. Huann et al [3] presented a 2nd order sliding mode controller combined with fuzzy control to suspend a magnetic ball and to satisfy the required robustness by rejecting the external disturbance and compensating the parameters variations.

The aim of this work is to design a simple robust controller for magnetic levitation system. This controller can achieve the robustness and a desirable time response specifications for the system with the presence of wide range of system parameters change and disturbance.

2. System Description and Mathematical Model

The magnetic levitation system considered in this work is consisting of a ferromagnetic ball suspended in a voltage-controlled magnetic field. Figure (1) shows the diagram of magnetic levitation system [4].

Electromagnetic units play an important role in magnetic levitation control. They allow measured signals to be transferred to the personal computer (PC) via an input/output (I/O) card. The Analogue Control Interface is used to transfer control signals from the PC to magnetic levitation and back [5]. The mechanical and electrical units provide a complete control system setup as presented in Figure (2).

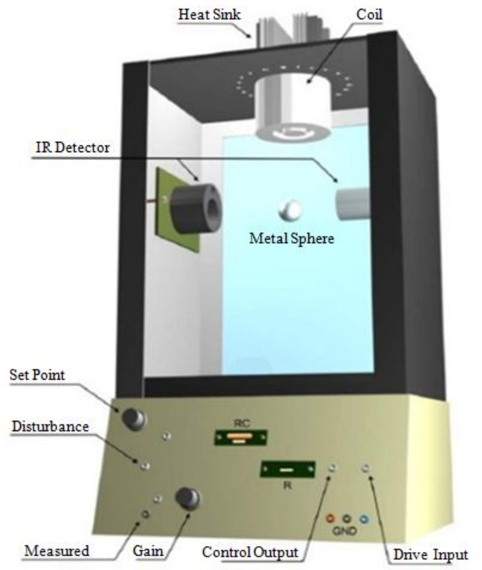

Figure (1): Electromagnetic levitation system [4].

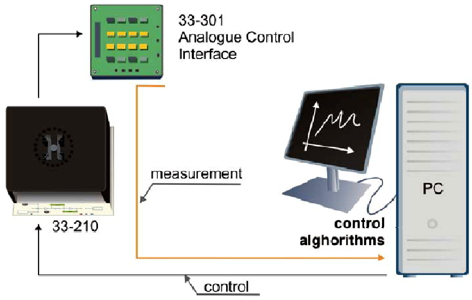

Figure (2): Magnetic levitation control system [4].

On the other hand, the magnetic levitation system consists of an electromagnetic, a metal sphere and an infra-red sphere position sensor. The magnetic ball suspension system can be categorized into two parts: mechanical system part and electromagnetic system part.

The mechanical part of the magnetic levitation system is considered at first, where the free body diagram of ferromagnetic ball suspended by balancing the electromagnetic force f_{em} and the force due to gravity f_g is shown in Figure (3).

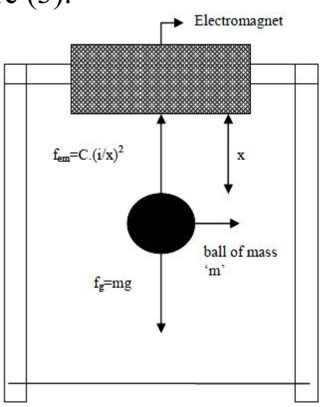

Figure (3): Free Body diagram of magnetic levitation system [4].

Net force f_{net} acting on the ball is given by Newton's 3rd law of motion while neglecting friction, drag force of the air is given by [6]:

$$f_{net} = f_g - f_{em} \qquad (1)$$

$$m\ddot{x} = mg - f_{em} \qquad (2)$$

where $f_{em} = c\,\frac{i^2}{x^2}$ and c is a constant depending on the coil (electromagnet) parameters, i is the current in the coil of electromagnet and x is the position of the ball. f_{em} denotes the magnetic force generated by the coil. At equilibrium state the magnetic becomes equal to the gravitational force on the object and the acceleration of the object is zero. Consequently, Equation (2) will be [6]:

$$mg = c\,\frac{io^2}{xo^2} \qquad (3)$$

where i_o is the current in the coil of electromagnet at equilibrium point, x_o is the position of the ball at equilibrium point, m is the metal sphere mass and g is the gravitational force. After substituting the values of m, g, and x_o in Equation (3), c will equal to 2.29×10^{-5}.

The magnetic ball position will be influenced by the inductance of the electromagnet coil. Also the levitating point between the electromagnetic force and gravity is inherently unstable. This problem can be solved by linearizing the nonlinear electromagnetic force.

At equilibrium state, the following equation is obtained [6]:

$$m\ddot{x} = c\,\left(\frac{2io^2}{xo^3}\right) x - c\,\left(\frac{2io}{xo^2}\right) i \qquad (4)$$

and by Laplace transform, the relationship between $X(s)$ and $I(s)$ is obtained as:

$$ms^2X(s) = c\,\left(\frac{2i_o^2}{x_o^3}\right) X(s) - c\,\left(\frac{2i_o}{x_o^2}\right) I(s) \qquad (5)$$

and the resulting transfer function for the mechanical part is:

$$\frac{X(s)}{I(s)} = \frac{-\,c\,\left(\frac{2i_o}{x_o^2}\right)}{\left(ms^2 - c\,\left(\frac{2i_o^2}{x_o^3}\right)\right)} \qquad (6)$$

On the other hand, the electromagnetic part of the system is shown in Figure (4). After applying Kirchhoff's voltage and current laws, the following equations are developed:

$$e_{in} - e_{out} = L\frac{di_L}{dt} \quad (7)$$

$$e_{out} = i_R R \quad (8)$$

$$e_{in} - L\frac{di_L}{dt} - e_{out} = 0 \quad (9)$$

$$i_L = i_R + i_{out} = i_R + 0 = i \quad (10)$$

$$e_{in} - L\frac{d}{dt}\left(\frac{e_{out}}{R}\right) - e_{out} = 0 \quad (11)$$

Taking Laplace transform yields:

$$\left(\frac{L}{R}s + 1\right) E_{out} = E_{in} \quad (12)$$

$$\frac{iR\ R}{E_{in}} = \frac{1}{\frac{L}{R}s+1} \quad (13)$$

$$\frac{i}{E_{in}} = \frac{\frac{1}{R}}{\frac{L}{R}s+1} \quad (14)$$

The resulting transfer function of the electromagnetic part is:

$$\frac{I(s)}{E_{in(s)}} = \frac{\frac{1}{R}}{\frac{L}{R}s+1} \quad (15)$$

where $I(s)$ is the current passes through the inductance and the resistance according to Equation (10).

Consequently, the total model of the magnetic levitation system can be expressed by:

$$\frac{X(s)}{E_{in}(s)} = \frac{\frac{-\left(\frac{2io}{xo^2}\right)c}{R}}{\frac{mL}{R}s^3 + ms^2 - c\left(\frac{2io^2}{xo^3}\right)\frac{L}{R}s - c\left(\frac{2io^2}{xo^3}\right)}$$

...(16)

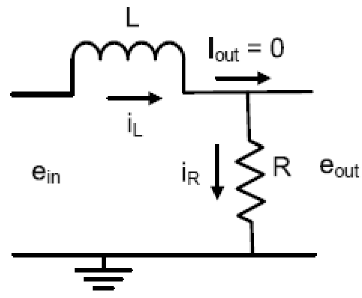

Figure (4): Magnetic levitation system (electromagnetic part).

On the other hand, the magnetic levitation system can be expressed as a state space model as:

$$\begin{bmatrix}\dot{x}_1\\ \dot{x}_2\\ \dot{x}_3\end{bmatrix} = \begin{bmatrix} 0 & 1 & 0\\ 0 & 0 & 1\\ \frac{c\left(\frac{2io^2}{xo^3}\right)R}{mL} & \frac{c\left(\frac{2io^2}{xo^3}\right)}{m} & -\frac{R}{L}\end{bmatrix}\begin{bmatrix}x_1\\ x_2\\ x_3\end{bmatrix} + \begin{bmatrix}0\\ 0\\ \frac{-\left(\frac{2io}{xo^2}\right)}{mL}\end{bmatrix}E_{in}$$

...(17)

$$x(t) = \begin{bmatrix}\frac{-\left(\frac{2io}{xo^2}\right)}{R} & 0 & 0\end{bmatrix}\begin{bmatrix}x_1\\ x_2\\ x_3\end{bmatrix} \quad (18)$$

where,

x_1 (t) = $\bar{x}$, (position of the metal sphere ball)

x_2 (t) = $\dot{\bar{x}}$, (velocity of the metal sphere ball)

x_3 (t) = $\ddot{\bar{x}}$, (acceleration of the metal sphere ball)

The nominal values of the system parameters and their variation range are illustrated in Table (1).

Table (1): List of system parameters and their variation ranges [6].

Parameter	**Minimum value**	**Nominal value**	**Maximum value**
R	17 *Ω*	34 *Ω*	51 *Ω*
L	77×10^{-3} *H*	154×10^{-3}	231×10^{-3}
M	0.004 *kg*	0.008 *kg*	0.012 *kg*
G	-	9.81 *m/s*^{2}	-
i_o	-	0.31 *Amp*	-
x_o	-	0.0053 *m*	-

3. Uncertainty Model Construction

If an accurate gain and phase uncertainty regions have been presented for a particular system, such shapes will be difficult to work with. *i.e.* their mathematical description is complicated. A common solution is to replace these complicated structured uncertainty regions with circular disk unstructured region at every frequency. The reason for using disk is that it can be easily described in the complex plane. On the other hand, the plant with structured uncertainty can be expressed in terms of unstructured multiplicative uncertainty by selecting a set of nominal plants to evaluate the disk of uncertainty as in the following Equation [7]:

$$G_p(s) = G_n(s)\,(1+W_m\,\Delta_m) \qquad (19)$$

For Δ_m =1, the multiplicative uncertainty function, W_m can be expressed as:

$$W_m(s) = \frac{G_p(s) - G_n(s)}{G_n(s)} \qquad (20)$$

where $G_p(s)$ is the uncertain parameters of the system, $G_n(s)$ is the nominal plant. Thus W_m represents the frequency response of all plants resulting from the variation of system parameters. The procedure for uncertainty model construction using curve fitting method is summarized by the following steps:

1. Plotting the frequency response of the system with all uncertain parameters.

2. Obtaining the largest magnitudes of the frequency response plot of the uncertain system.

3. Plotting a curve that fits the large magnitudes points.

4. Selecting the order of the curve that fits the large magnitudes points.

5. The uncertainty model can be constructed after choosing a suitable order of the large magnitudes curve.

In this work, the uncertainty model has been determined for 50% change in system parameters. The obtained uncertainty model is:

$$W_m(s) = \frac{0.1087\,s^2 + 0.0133\,s + 0.001353}{s^2 + 0.1672\,s + 0.02844} \qquad (21)$$

Figures (5) and (6) show the frequency response characteristics of the obtained uncertainty model and its inverse.

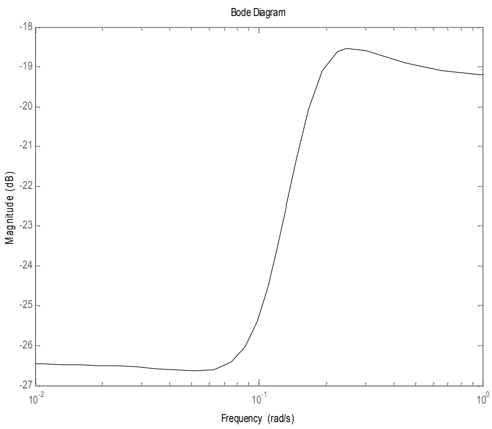

Figure (5): Frequency response characteristics of the uncertainty model (W_m).

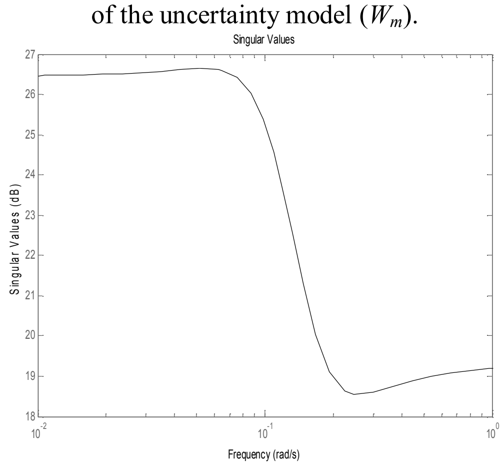

Figure (6): Frequency response characteristics of the inverse of uncertainty model (W_m^{-1}).

4. H$_\infty$ Control Problem and Weighting Functions

The H$_\infty$ optimal control design technique deals with the problem of robustness by deriving controllers, which maintain system response, and error signals to within prescribed tolerance, despite the presence of uncertainty and disturbance in the system [8].

The performance analysis is defined in the frequency domain in terms of sensitivity function $S(s)$, and complementary sensitivity function $T(s)$. These functions can be expressed as [8, 9]:

$$S(s) = (I + G_n(s)K(s))^{-1}$$
$$T(s) = G_n(s)K(s)\,(I + G_n(s)K(s))^{-1} \quad (22)$$

where $G_n(s)$ is the nominal plant, $K(s)$ is the controller to be designed. The relation between the sensitivity function and the complementary sensitivity function is:

$$S(s) + T(s) = 1 \quad (23)$$

The robust optimal control consisting of finding a stabilizing controller $K(s)$, such that the H$_\infty$ -norm of the sensitivity function $\|S(s)\|_\infty$ and the complementary sensitivity function $\|T(s)\|_\infty$ are to be minimized. The robust H$_\infty$ condition is satisfied when the following conditions are satisfied [6, 8]:

$$|W_p(s)\,S(s)| < 1 \quad (24)$$

$$|W_m(s)\,T(s)| < 1 \quad (25)$$

On the other hand, to improve the performance of the plant to follow some given reference signal and to reject the disturbance by designing a controller, a suitable selection of performance and control weighting functions is required. This procedure of the selection is not easy and often needs many iterations and fine tuning and it is hard to find a general formula for the weighting functions that can work in every case. In this work the selected structures of the performance and control weighting functions respectively are [6]:

$$W_p(s) = \frac{(\frac{s}{\sqrt{M_s}} + w_b)^2}{(s + w_b\sqrt{e_{ss}})^2} \quad (26)$$

where w_b is the minimum acceptable frequency bandwidth (for disturbance rejection), and M_s is the maximum peak magnitude of sensitivity $|S(jw)|$ and e_{ss} is the allowed steady state error.

$$W_u(s) = \frac{S + (\frac{w_{bc}}{M_u})}{\varepsilon S + w_{bc}} \quad (27)$$

where M_u is the maximum peak magnitude of $|K(s)S(jw)|$, ε is a small value and w_{bc} is the controller bandwidth.

5. Basic H$_\infty$ Controller Design

The transformation into standard configuration can be done using Lower Fractional Transformation (LFT) technique: LFT is a technique which specifies grouping signals into sets of external inputs (w) and outputs (z), input to the controller (v) and output from the controller (control signal u) [8]. Figures (7) and (8) show the lower fractional transformation block and the block diagram of the system with weighting functions respectively.

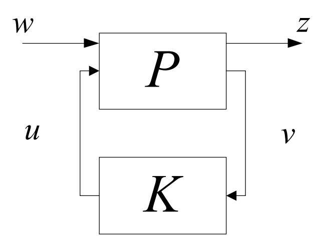

Figure (7): Lower fractional transformation (LFT).

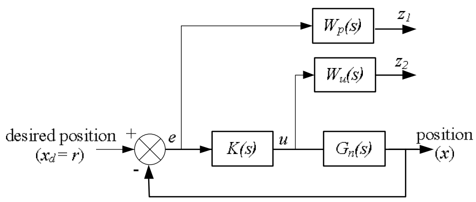

Figure (8): Block diagram of the system with weighting functions.

The relationship between z and w can be expressed as:

$$z(s) = \begin{bmatrix} W_p - G_n W_p\, K\, (I + G_n K)^{-1} \\ W_u\, K\, (I + G_n K)^{-1} \end{bmatrix} w(s)$$
...(28)

To add the uncertainty model to the system, the Lower Fractional Transformation (LFT) is transformed to the Upper Fractional Transformation (UFT) by obtaining N which is equal to $F_l\,(P,K)w$ as shown in Figure (9) [6].

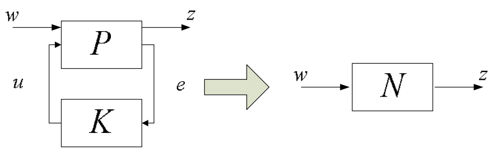

Figure (9): Lower fractional transformation (LFT) to upper fractional transformation (UFT).

The H$_\infty$ control design deals with both structured and unstructured uncertainty. However, the design scheme that involving unstructured uncertainty gives more control over the system (since it can cover unmodeled system dynamics at high frequencies) [8]. Figure (10) shows the block diagram of the system with the multiplicative uncertainty model. The input signal d represents the external disturbance.

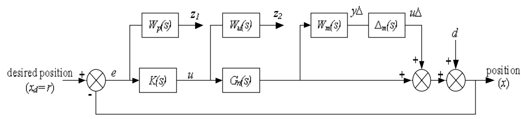

Figure (10): Block diagram of system with weighting functions and uncertainty.

The uncertainty model is added to the system as shown in Figure (11) to form the Upper Fractional Transformation (UFT).

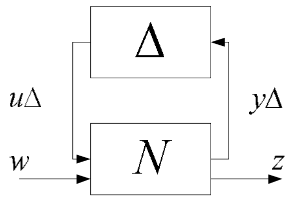

Figure (11): Upper fractional transformation (UFT).

The transfer function with uncertainty that relates w to z can be found using Upper Fractional Transformational (UFT) function as:

$$N(s) = \begin{bmatrix} -W_m T & W_m T & -W_m T \\ -W_p S & W_p S & -W_p S \\ -W_u KS & W_u KS & -W_u KS \end{bmatrix} w(s)$$
...(29)

In the H$_\infty$ controller design the cost function to be minimized is:

$$\|F_u(N,\Delta)\|_\infty < \gamma \qquad (30)$$

where γ represents the bound to be minimized.

The performance and control weighting functions used in the design of basic H$_\infty$ controller are set by trial and error to meet the required robust stability and performance. The selected weighting functions are:

$$W_p(s) = \frac{0.3s^2 + 22s + 18000000}{61s^2 + 100s + 10} \qquad (31)$$

$$W_u(s) = \frac{3s^3 + 0.9s^2 + 0.6s + 0.06}{0.6\, s^3 + s^2 + 2s + 1} \qquad (32)$$

The objective of the H_∞ control is to find the controller $K(s)$ that internally stabilizes the system such that the cost function in Equation (30) is minimized. The H_∞ control minimizes the cost function in Equation (30) using γ-iteration to find the stabilizing controller such that the cost function in Equation (30) is minimized. This means that the conditions in Equations (24) and (25) are satisfied.

The interval of γ iteration is selected between 0.1 and 10 and the obtained suboptimal H_∞ controller for the magnetic levitation system is:

$$K(s) = \frac{-1286\, s9 - 8.324e07\, s8 - 3.582e22\, s7 - 1.57e25\, s6 - 2.299e27\, s5 - 1.439e29\, s4 - 3.378e30\, s3 - 5.698e30\, s2 - 1.069e31\, s - 5.228e30}{s^{10} + 9.293e04\, s^9 + 4.323e09\, s^8 + 1.246e14\, s^7 + 2.23218\, s^6 + 2.051e22\, s^5 + 3.495e23 s^4 + 3.005e23\, s^3 + 1.255e24\, s^2 + 7.515e23\, s + 7.502e20}$$
...(33)

6. H_∞ based Robust PID Controller Design

The selected PID controller is considered to provide a suitable loop transfer function and to satisfy H_∞ norm specifications. The PID controller is commonly used because of making PID controllers with automatic tuning, automatic generation of gain schedules and continues adaptation. The PID structure used in this work is:

$$K(s) = K_p + \frac{K_i}{s} + K_d \frac{n}{1+\frac{n}{s}} \qquad (34)$$

where K_p, K_i and K_d are the controller parameters, n is a filter coefficient. These parameters are tuned such that the closed loop system is asymptotically stable, and the required robust performance specifications are achieved.

In this work, the cost function that will be used to be minimized is:

$$J_{min} = \| W_m T + W_p S \|_\infty + \int_0^{t_f} |e(t)|\, dt$$
...(35)

where, t_f is chosen to be the settling time of the system and $e(t)$ is the error signal of the system.

This cost function is a combination of H_∞ -norm specifications and time domain specifications represented by the performance index (IAE) integral of absolute value of error. That is the proposed cost function is wanted to meet multiple design requirements.

6.1 Genetic Algorithm (GA) Based Controller Design

Genetic Algorithms (GA) are stochastic global search methods based on the mechanics of natural selection and natural genetics. They are iterative methods, widely used in optimization problems in several branches of the sciences and technologies [9].

The most crucial step in applying GA is to choose the objective functions that are used to evaluate fitness of each chromosome. The cost function in Equation (35) is used to be minimized using GA method. The PID controller is used to minimize the error signal, or we can define more rigorously, in the term of error criteria: to minimize the value of cost function in Equation (35). The performance index of the chromosome is defined as [9]:

$$Fitness\ value = \frac{1}{Performance\ index} \qquad (36)$$ (23)

After many simulation tests, it was found that the maximum number of iterations of (1000) iterations was sufficient to obtain the best minimization of the cost function where any other increasing in the number of iterations did not improve the convergence of the GA significantly. The population size was selected to be 10, the selection function has been selected to be "Normalized geometric function", the probability of selecting the fitness chromosome of each generation was set to be 0.32, "Arithmetic crossover" was chosen as the crossover procedure, and "Multi non-uniformly mutation" was used as mutation operator where the total number of mutations was normally set to 32.

The obtained PID controller and weighting performance function using GA respectively are:

$$K(s) = \frac{-1.891e06s^2 - 3.685e07s - 3.581e07}{s^2+4255\,s} \quad ...(37)$$

where
K_p = -8659, K_i = -8417, K_d = - 442.4, and n = 4255.

$$W_p(s) = \frac{0.001s^2 + 0.002s + 0.02}{0.01s^2 + 0.03s + 0.01} \qquad (38)$$

The overall block diagram of the system with Genetic Algorithm (GA) tuning process of PID controller are shown in Figure (12), where d is an external disturbance.

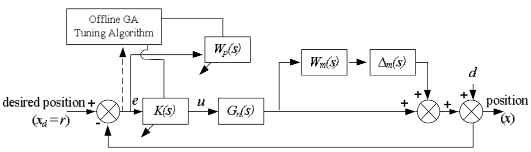

Figure (12): The overall block diagram of the controlled system.

6.2 Particle Swarm Optimization (PSO) Based Controller Design

Particle Swarm Optimization (PSO) is a stochastic population based optimization algorithm, firstly introduced by Kennedy and Eberhart in 1995. In PSO algorithm, each member of the population is called a ‘‘particle’’, and each particle ‘‘flies’’ around in the multidimensional search space with a velocity, which is constantly updated by the particle’s own experience and the experience of the particle’s neighbors or the experience of the whole swarm [10]. The basic concept of PSO technique lies in accelerating each particle towards its P_{best} (previous best position) and G_{best} (global best position) locations, with a random weighted acceleration at each time step. The velocity and position of the particle are changed according to the following velocity and position equations respectively [11]:

$$V_i^{t+1} = w \times V_i^t + C_1 \times U \times (X_i^b - X_i^t) + C_2 \times U \times (X_i^g - X_i^t) \quad (39)$$

$$X_i^{t+1} = X_i^t + V_i^{t+1} \qquad (40)$$

where V_i^t is the particle velocity, X_i^t is the current particle position, w is the inertia weight, X_i^b and X_i^g are the best value and the global best value respectively, U is a random function between 0 and 1, C_1 and C_2 are learning factors [12].

The PSO algorithm can be summarized by the following steps:

1. Creating a ‘population’ of agents (called particles).

2. Evaluating each particle’s position according to the objective function.

3. If a particle’s current position is better than its previous best position, it will update it.

4. Determining the best particle (according to the particle's previous best positions).

5. Updating particles' velocities according to Equation (39).

6. Moving the particles to their new positions according to Equation (40).

7. Going to step 2 until the stopping criteria are satisfied.

8. Evaluating each particle's position according to the objective function.

In this work the cost function to be minimized using PSO method is expressed in Equation (35).

After many simulation tests, it was found that the maximum number of iterations of (1000) is sufficient iterations to obtain the best minimization of the cost function, where any other increase in the number of iterations did not improve the convergence of the PSO algorithm significantly. On the other hand, for carrying out the design of the controller using PSO, the PSO parameters have been selected as: swarm size=10, C_1= C_2 = 2, w = 2. The obtained PID controller and weighting performance function using PSO method respectively are:

$$K(s) = \frac{-113200s^2 - 4.333e06s - 4.193e07}{s^2 + 896\,s} \quad \ldots(41)$$

where
K_p = -4784, K_i = -46798, K_d = -121, and n = 896.

$$W_p(s) = \frac{0.001s^2 + 0.002s + 0.02}{0.01s^2 + 0.03s + 0.01} \quad (42)$$

The overall block diagram of the system with PSO tuning algorithm is shown in Figure (13).

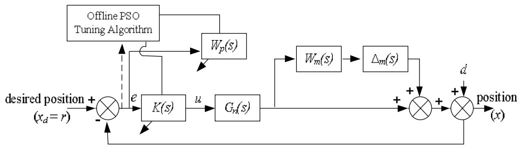

Figure (13): The overall block diagram of the controlled system.

7. Results and Discussion

Figure (14) shows the time response specifications of open loop and closed loop system without controller. It is clear that the system is highly unstable and the design of suitable controller is required.

a. Basic H$_\infty$ Controller Results

The robust stability and performance can be achieved as shown in Figures (15) and (16) respectively that explain the resulting sensitivity and complementary sensitivity functions. From these figures it is shown that the magnitudes of sensitivity S, and complementary sensitivity functions T, are always less than the magnitude of the inverse of uncertainly function W_p, and performance weighting function W_m, respectively. This shows that the condition of robust stability and performance in Equations (24) and (25) has been satisfied. Figure (17) shows the time response specifications of the resulting control signal using basic H$_\infty$ controller. The obtained time response specifications can be shown in Figure (18). The obtained time response specifications are: rise time t_r = 0.08 s and settling time t_s = 0.13 s.

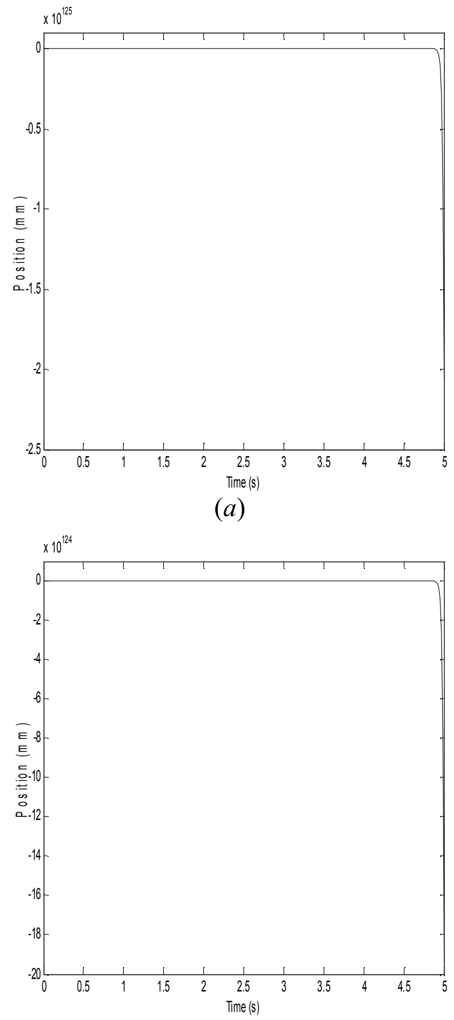

(*a*)

(*b*)

Figure (14): Time response specifications of the system without controller. (*a*) open loop. (*b*) closed loop.

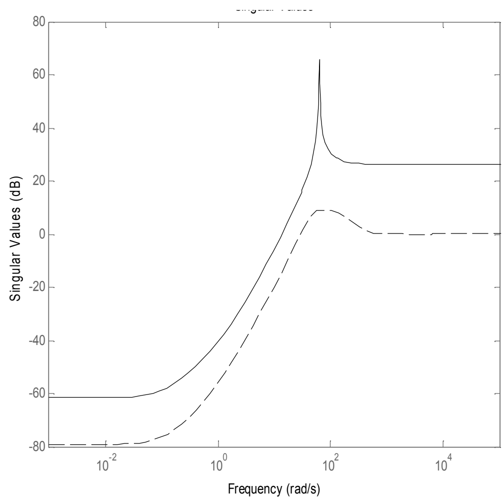

Figure (15): Singular values of the sensitivity function *S* (*dotted*) and the corresponding weighting function W_p^{-1} (*solid*) using basic H_∞ controller.

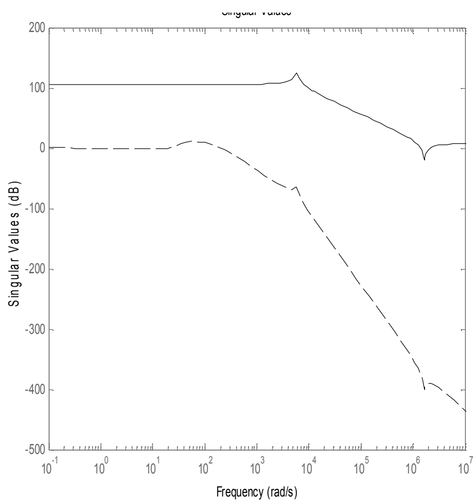

Figure (16): Singular values of the complementary sensitivity function *T* (*dotted*) and the corresponding uncertainty function W_m^{-1} (*solid*) using basic H_∞ controller.

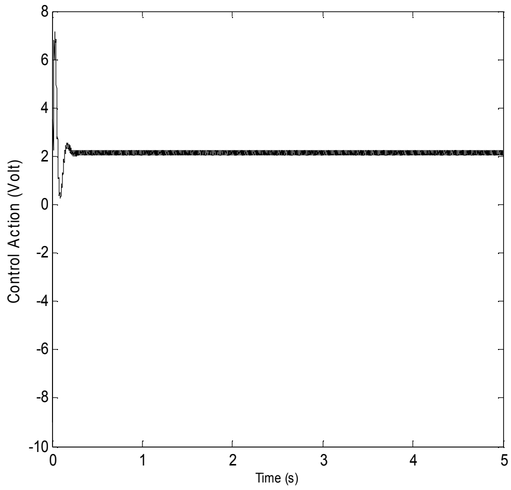

Figure (17): The resulting control signal using basic H_∞ controller.

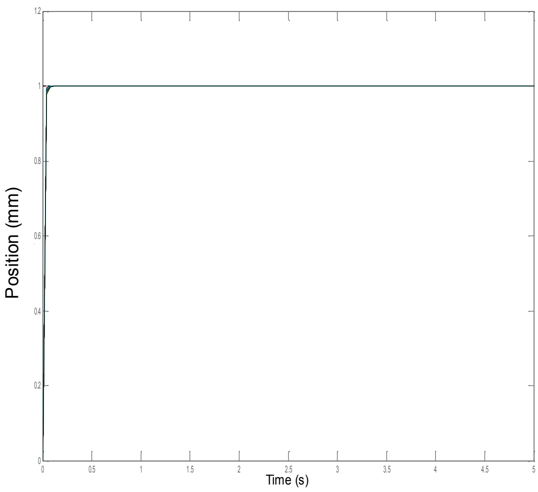

Figure (18): Closed loop time response specifications of the system using basic H_∞ controller.

b. Robust GAPID and PSOPID Controllers Results

To demonstrate the effectiveness of the proposed robust GAPID and robust PSOPID controllers, extensive tests on the magnetic levitation system have been performed as shown in Figures (19) to (22). From these figures it can be seen that the magnitudes of sensitivity and complementary sensitivity functions are less than the magnitudes of the inverse of performance and uncertainty weighting functions for all frequencies and for both robust GAPID and PSOPID controllers. This means that the robust stability and robust performance conditions in Equations (24) and (25) have been achieved.

On the other hand, the obtained time response specifications for robust GAPID controller can be shown in Figure (23), where M_p = 28%, t_p = 0.23 *s,* t_s = 3.4 *s* and t_r = 0.12 *s*, and the obtained time response specifications for robust PSOPID controller can be shown in Figure (24) where M_p = 18%, t_p = 0.2452 *s*, t_s = 0.8223 *s* and t_r = 0.12 *s*. Furthermore, the time response specifications of the control efforts using GAPID and PSOPID controllers are shown in Figures (25) and (26) respectively. The step response of the uncertain system with GAPID controller and PSOPID controller are shown in Figures (27) and (28) respectively.

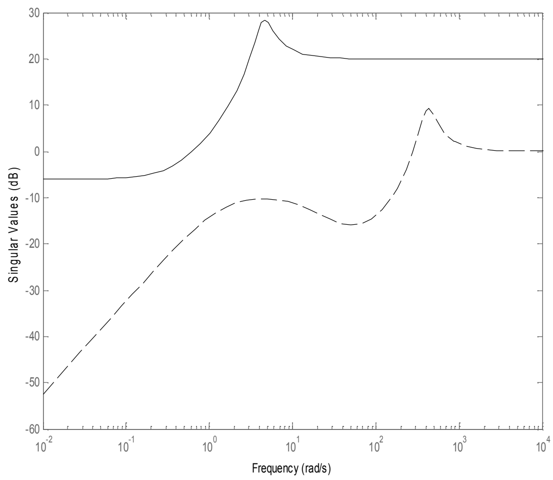

Figure (19): Singular values of the sensitivity function S (*dotted*) and the corresponding weighting function W_p^{-1} (*solid*) using robust GAPID controller.

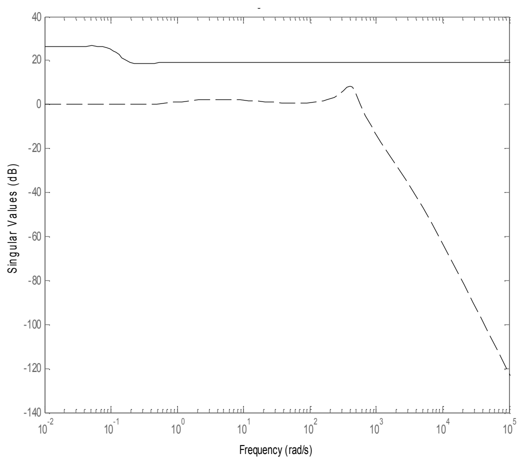

Figure (21): Singular values of the complementary sensitivity function T (*dotted*) and the corresponding uncertainty function W_m^{-1} (*solid*) using robust GAPID controller.

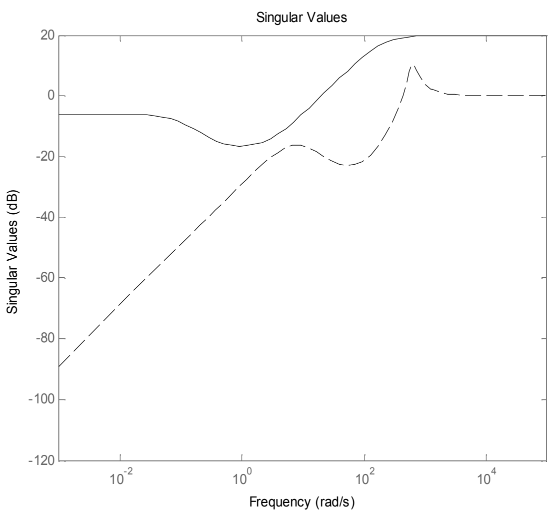

Figure (20): Singular values of the sensitivity function S (*dotted*) and the corresponding weighting function W_p^{-1} (*solid*) using robust PSOPID controller.

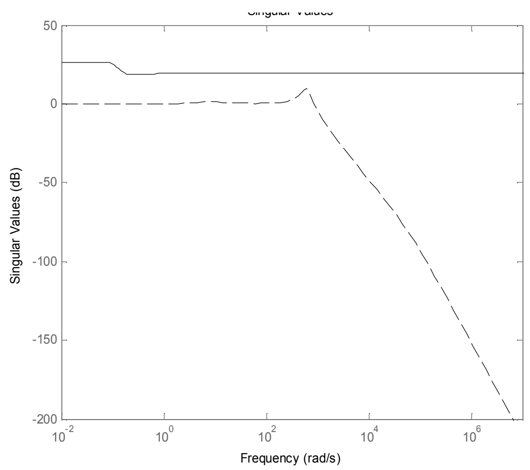

Figure (22): Singular values of the complementary sensitivity function T (*dotted*) and the corresponding uncertainty function W_m^{-1} (*solid*) using robust PSOPID controller.

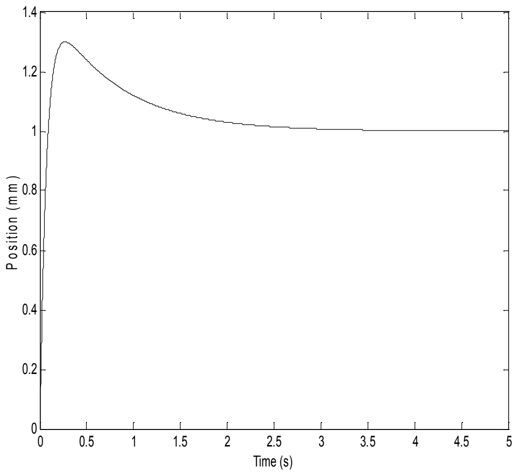

Figure (23): Closed loop time response specifications for the designed robust GAPID controller.

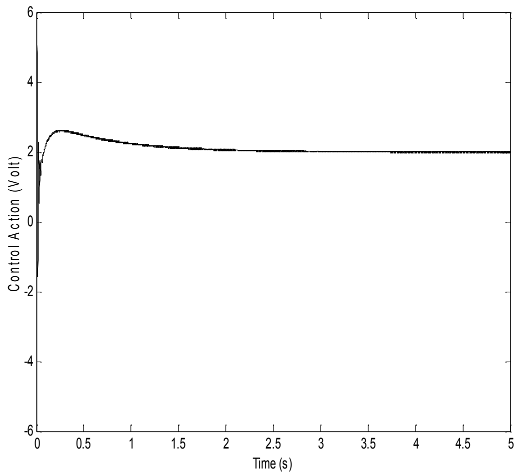

Figure (25): The resulting control signal for the designed robust GAPID controller.

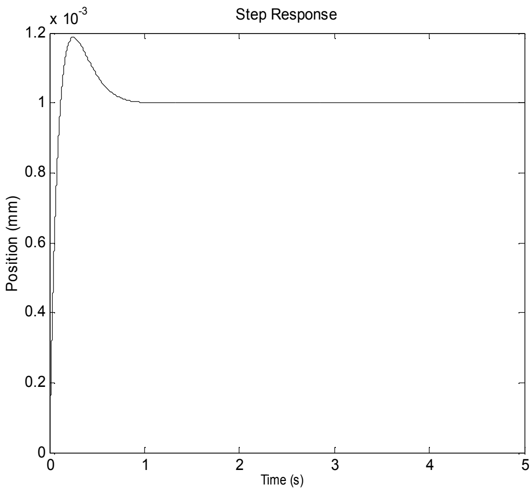

Figure (24): Closed loop time response specifications for the designed robust PSOPID controller.

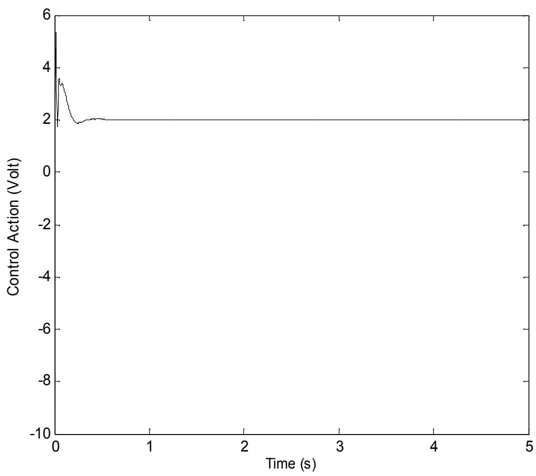

Figure (26): The resulting control signal for the designed robust PSOPID controller.

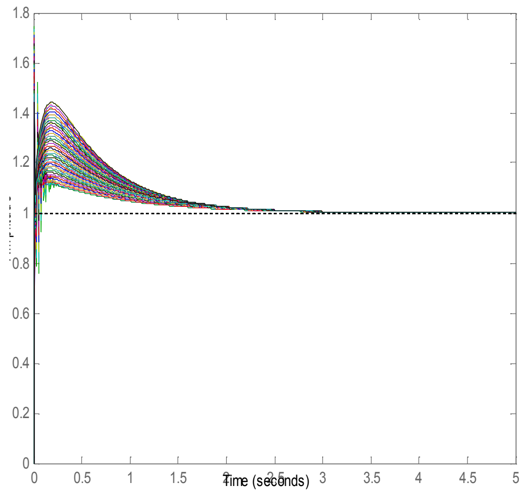

Figure (27): The step response of the uncertain system with GAPID controller.

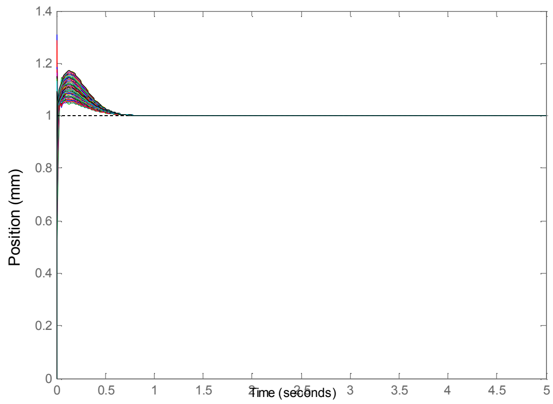

Figure (28): The step response of the uncertain system with PSOPID controller.

On the other hand, to show the robustness of the proposed robust PSOPID controller, several tests on the magnetic levitation system with applying different disturbances signals have been performed as shown in Figures (29) to (34). A sine wave disturbance of amplitude equal to 0.008, sample pulse of amplitude equal to 0.001 and step signal with (amplitude equal to 0.001, phase=0, period=10 and pulse width=10) and step signal with amplitude equal to 0.008 have been applied to the system. From these results, it can be noted that the robust PSOPID controller can effectively compensate the disturbances. Further, the system can converge to the desired position without any dynamic oscillation in case of sinusoidal and step disturbances and with small effect in case of sample pulse disturbance.

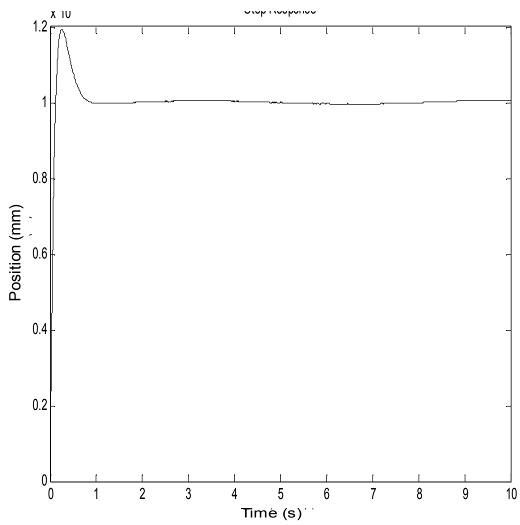

Figure (29): Time response specifications of the system using robust PSOPID controller with *d*=0.008sint.

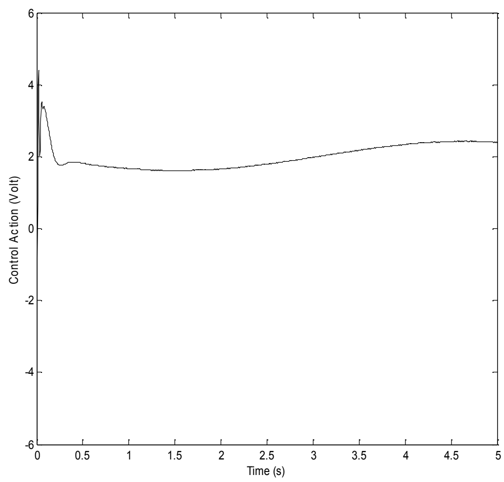

Figure (30): The resulting control signal using robust PSOPID controller with *d*=0.008sint.

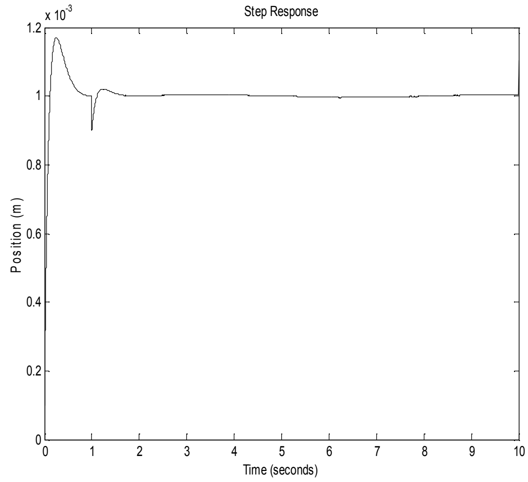

Figure (31): Time response specifications of the system using robust PSOPID controller with *d*=0.008sint+pulse signal having (*amplitude*=0.001, *phase*=0, *period*=10 and *pulse width*=10).

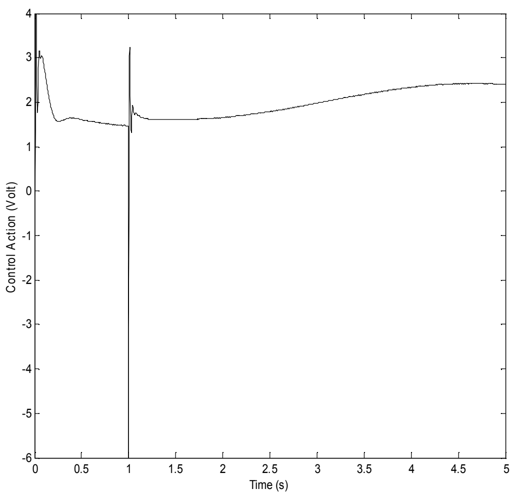

Figure (32):The resulting control signal using robust PSOPID controller with *d*=0.008sint+pulse signal having (*amplitude*=0.001, *phase*=0, *period*=10 and *pulse width*=10).

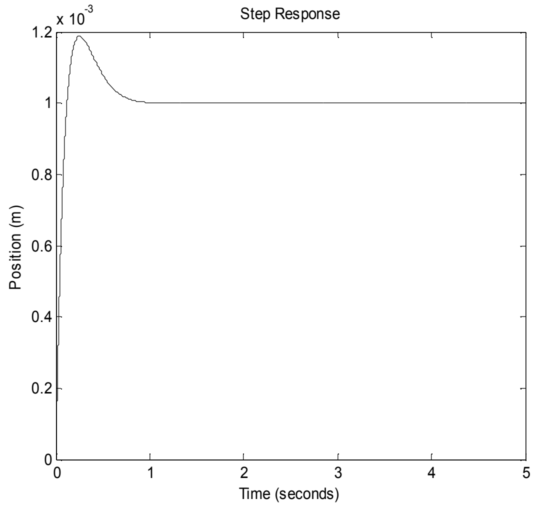

Figure (33): Time response specifications of the system using robust PSOPID controller with *d*=0.008 step signal.

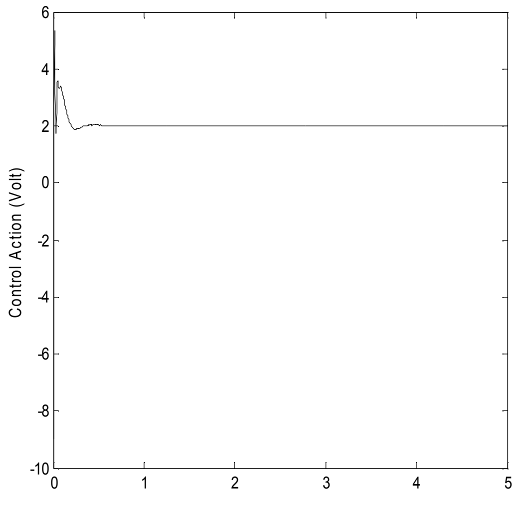

Figure (34):The resulting control signal using robust PSOPID controller with *d*=0.008 step signal.

8. Conclusions

H_∞ technique is a popular robust feedback control strategy that is used to achieve the system objectives in the presence of system uncertainties and/or disturbance. On the other hand, the magnetic levitation system is one of the high non linearity and uncertain systems, therefore, it is an important step to design a simple robust controllers based on H_∞ technique. The first designed controller is the basic H_∞ controller which is a powerful technique to design a robust controller. The disadvantage of this method is that the design procedure is complex and difficult to fine tuning the weighting functions in order to achieve the robust performance and robust stability. Furthermore, the resulting basic H_∞ controller is high order.

On the other hand, the use of GA and PSO method to design robust PID controller, simplifies the design procedure of H_∞ controller and overcomes the difficulty of the resulting high order controller. Further, the design of robust controller using specific structure controllers like PID is very efficient and it can effectively compensate the uncertain system with a wide range of system parameters change. Finally, the proposed robust PSOPID controller can achieve the required robustness with a desirable time and frequency responses specifications.

References

[1] B. Anselmo and S. R. Moura, "H_2 and H_∞ Control for Magnetic Levitation Vehicle", IEEE Control Systems, Vol. 18, No. 4, pp. 18-25, August, 1998.

[2] A. Kumar, M. K. Panda, S. Kundu and V. Kumar, "Designing of an Interval Type-2 Fuzzy Logic Controller for Magnetic Levitation System with Reduced Rule Base", IEEE, 12th International Conference on Computing, Communications and Networking Technologies, Coimbatore, India, July, 2012.

[3] H. K. Chiang, C. C. Fang and G. W. Chen, "Second Order Siding Mode Control with Fuzzy Compensator for a Magnetic Levitation System", IEEE, Second International Conference on Digital Manufacturing and Automation, Hunan, China, August, 2011.

[4] I. Ahmad and M. A. Javaid, "Nonlinear Model & Controller Design for Magnetic Levitation System", Recent Advances in Signal Processing, Robotics and Automation, University of Engineering & Technology, Taxila, Pakistan, 2012.

[5] "Magnetic Levitation Control 33-942 S", Feedback Instruments Ltd., UK, 2009.

[6] R.A. Jose and A.S. Gadhi, "Development and Control of a Non Linear Magnetic Levitation System", International Journal on Theoretical and Applied Research in Mechanical Engineering (IJTARME), pp. 2319-3182, Vol. 2, No. 1, 2013.

[7] D. Richard "Modern Control System", Upper Saddle River, New Jersey: Prentice Hall Inc., 2001.

[8] J. Zhang, L. He, E. Wang and R. Gao, "Robust Active Vibration Control of Flexible Structures Based on H_∞ Control Theorem", International Workshop, China, Vol. 978, No. 1, pp. 4244-3894, September, 2009.

[9] J. S. Kim, J. H. Kim, J. M. Park, S. M. Park, W. Y. Choe and H. Heo, "Auto Tuning PID Controller based on Improved Genetic Algorithm for Reverse Osmosis Plant", World Academy of Science, Engineering and Technology Vol. 2, No. 11, 2008.

[10] X. Yang, J. Yuan and H. Mao, "A Modified Particle Swarm Optimizer With Dynamic Adaptation", Applied Mathematics and Computation, Vol. 189, No. 2, pp. 1205-1213, 2007.

[11] H. I. Ali, Y. K. Abbas and A. M. Mahmood, "PSO Based PID Controller Design for a Precise Tracking of Two-Axis Piezoelectric Micro Positioning Stage", Engineering and Technology Journal, Vol. 31, Part (*A*), No. 17, pp. 2385-2397, 2013.

[12] H. A. Jabber, "Design of Optimal Controller using H_2 Algebraic Methods", M.Sc. Thesis, University of Technology, Control and Computer Engineering Department, November, 2000.